

Article

Bio-Inspired Mechano-Sensor Based on the Deformation of Slit Wake

Kejun Wang, Lei Gao, Yuecheng Gui, Zezhong Lu, Deshan Wang, Jiaqiang Li * and Qian Wang *

School of Mechanical and Electric Engineering, Soochow University, Suzhou 215021, China; kjwang@suda.edu.cn (K.W.); 20215229100@stu.suda.edu.cn (L.G.); 20195229009@stu.suda.edu.cn (Y.G.); 20215229107@stu.suda.edu.cn (Z.L.); wangwangdeshan@163.com (D.W.)

* Correspondence: lijiaq@suda.edu.cn (J.L.); qianwang@suda.edu.cn (Q.W.)

Abstract: Internal mechano-sensors, as an indispensable part of the proprioceptive system of intelligent equipment, have attracted enormous research interest because of their extremely crucial role in monitoring machining processes, real-time diagnosis of equipment faults, adaptive motor control and so on. The mechano-sensory structure with signal-transduction function is an important factor in determining the sensing performance of a mechano-sensor. However, contrary to the wide application of the cantilever beam as the sensory structure of external mechano-sensors in order to guarantee their exteroceptive ability, there is still a lack of an effective and widely used sensory structure to significantly improve the sensing performance of internal mechano-sensors. Here, inspired by the scorpion using the specialized slit as the sensory structure of internal mechano-sensilla, the slit is ingeniously used in the design of the engineered internal mechano-sensor. In order to improve the deformability of the slit wake, the hollowed-out design around the slit tail of biological mechano-sensilla is researched. Meanwhile, to mimic the easily deformed flexible cuticular membrane covering the slit, the ultrathin, flexible, crack-based strain sensor is used as the sensing element to cover the controllable slit wake. Based on the coupling deformation of the slit wake, as well as the flexible strain sensor, the slit-based mechano-sensor shows excellent sensing performance to various mechanical signals such as displacement and vibration signals.

Keywords: bio-inspired; slit; sensory structure; mechano-sensor



Citation: Wang, K.; Gao, L.; Gui, Y.; Lu, Z.; Wang, D.; Li, J.; Wang, Q. Bio-Inspired Mechano-Sensor Based on the Deformation of Slit Wake. *Appl. Sci.* **2022**, *12*, 4456. <https://doi.org/10.3390/app12094456>

Academic Editors: Ki-Hyun Kim and Deepak Kukkar

Received: 3 April 2022

Accepted: 25 April 2022

Published: 28 April 2022

Publisher's Note: MDPI stays neutral with regard to jurisdictional claims in published maps and institutional affiliations.



Copyright: © 2022 by the authors. Licensee MDPI, Basel, Switzerland. This article is an open access article distributed under the terms and conditions of the Creative Commons Attribution (CC BY) license (<https://creativecommons.org/licenses/by/4.0/>).

1. Introduction

Mechano-sensors are a kind of sensor that can convert a variety of mechanical signals (such as air/water flow, vibration, touch, acoustic signal, and so on) into electrical signals [1–4]. In the engineering field, mechano-sensors are important for engineering equipment to detect mechanical signals in the internal and external environment, because mechanical signals contain a lot of information for rehabilitation monitoring of advanced equipment, guiding the control of mechanical actuators, and precise motion control of intelligent robots in complex working conditions [5–8]. Recently, there has been an urgent need to further significantly improve the sensing performance of mechano-sensors. However, after decades of research, the mechano-sensors based on traditional design methods are quickly approaching their performance limits. Therefore, exploring novel strategies is very important for developing mechano-sensors with excellent performance such as ultra-high sensitivity, low power consumption, durability, and so on.

The signal-conduction sensory structure and signal-transduction materials are two major sensing elements of mechano-sensors [9–11]. The coupling design of the above two elements is key to achieving the optimal performance of various mechano-sensors. Because the mechanical signals cannot be directly received by signal-transduction materials, it first requires a highly specialized sensory structure to achieve the efficient collection of dispersed signals at the sites of nanoscale functional materials [12–14]. Obviously, it is one of the necessary ways for developing next-generation mechano-sensors by designing a

highly specialized sensory structure, which can achieve optimal signal transmission, for a corresponding mechanical signal. According to the classification of an exteroceptive and proprioceptive system, various types of mechano-sensors are divided into external mechano-sensors and internal mechano-sensors [15,16]. Specifically, the external mechano-sensors extending or protruding from the surface of the equipment mainly utilize exteroceptive capabilities through the direct detection of external stimuli containing air/fluid-flow signals and tactile signals [17,18]. For external mechano-sensors, various types of cantilever beams are widely utilized as the sensory structure because of its unique advantages in external mechanical-signal collection [19]. The internal mechano-sensors, as the important part of the proprioceptive system, are widely used to enhance the capability of the intelligent equipment to perceive the changes in their own state via detecting the internal mechanical stimulus that is generated in the object body [20]. Internal mechano-sensors with excellent comprehensive performance have attracted extensive attention because of their significant role in improving the proprioceptive capabilities of intelligent equipment [8,21]. However, contrary to the wide application of the cantilever beam as the sensory structure of external mechano-sensors, there is still a lack of an effective and widely used sensory structure for significantly improving the sensing performance of internal mechano-sensors. Obviously, it is an urgent problem to find a specific sensory structure that can be widely used and can significantly improve the performance of the internal mechano-sensor.

In nature, arachnids (such as the spider and scorpion), in which visual systems have been highly degraded, have evolved a variety of mechano-sensilla to meet their survival needs in a harsh natural environment [12,22]. Among various mechano-sensilla, the slit-based mechano-sensilla, as an important part of the proprioceptive system, are ingeniously used to sense the internal mechanical stimulation caused by walking and the external vibration signal [23,24]. The slit-based mechano-sensilla are distributed at the front of the basitarsus joint. When the external mechanical signal acts on the tarsus, the tarsus rotates around the end of metatarsus, which further causes the deformation of the slit-based mechano-sensilla due to the extrusion stress [25–29]. The slit-based mechano-sensilla are composed of bending slit units. The real-time observation result showed that the slit wake would periodically open and close under the alternating load [30,31]. In the engineering field, the “crack-shaped” slit is a typical defect owing to the significant stress amplification at the tip. Our previous research indicated that, for preventing the catastrophic fatigue fracture of the slit from the slit tip as well as ensuring the sensitivity of sensilla, the cuticular membrane with low bending stiffness and high tensile stiffness are ingeniously used to cover the slit wake. The ultrathin cuticular membrane is prone to bending deformation with the opening and closing of the slit wake. Obviously, the biological research clearly indicate that the slit-based mechano-sensilla provide a natural bio-inspired strategy for utilizing the slit as the sensory structure of an internal mechano-sensor in order to further significantly improve the sensing performance. Although the functional mechanism of the biological slit-based mechano-sensilla has been deeply researched, there has been a lack of bionic research on utilizing controllable slit as the sensory structure of the external mechano-sensor.

Herein, inspired by the open and close of the slit wake as well as the bending deformation of the cuticular membrane covering the slit wake in response to dynamic mechanical signals, we report a novel slit-based internal mechano-sensor. In the bio-inspired mechano-sensor, the flexible, ultrathin, crack-based mechano-sensitive strain sensor (FUCMSS) is utilized as the sensing element to cover the slit wake. With the deformation of the FUCMSS and slit wake, the mechanical signal is sensitively detected by efficiently collecting the mechanical signal and transforming it into a resistance signal. This work explains the design strategy of the slit-based mechano-sensor in detail and demonstrates great application foreground for utilizing the slit as the mechano-sensory structure of the next-generation mechano-sensor. The bio-inspired slit-based mechano-sensor may have a wide range of applications in the precise adaptive motion control of intelligent robots, the precise opera-

tion of actuators, as well as the real-time monitoring of the health and processing status of intelligent CNC machining equipment.

2. Materials and Methods

2.1. Fabrication of the “Hollow Out” Structures and Slit on the Solid Substrate

Transparent acrylic plate with a thickness of 2 mm was chosen as the substrate. The slit and the hollow structure around the slit tail were prepared on the acrylic plate using a laser cutting machine (HY-CFB01, HY Co., Liaocheng, China). The three-dimensional model of the solid substrate was built for finite-element (FEA) simulations. The commercial software Abaqus 6.14 (Dynamic, Explicit) was used to evaluate the influence of geometric parameters of the slit as well as the hollow structure on the deformation of slit.

2.2. Fabrication of the Flexible Crack-Based Strain Sensor

20 nm-thick Au film was deposited on the top of the flexible polyethylene terephthalate film with a thickness of 5 μm via sputtering (108 auto Cressington sputter coater). Then, a piece of sensing film with dimensions of 5 mm \times 20 mm ($l \times w$) was intercepted from the entire sample. Based on the home-made equipment, the nanoscale crack array was generated as the sensory structure by bending the sample, and the density of the crack was controlled by adjusting the curvature radii, loading magnitude, as well as the number of cycles. Cu leads were wired on top of the Au layer using Cu paste for the resistance measurement of the bio-inspired slit-based mechano-sensor. The FUCMSS covered the slit wake using epoxy resin.

2.3. Characterization of the Slit-Based Mechano-Sensors

A digital microscope with a super depth of field (Keyence, VHX-5000, Osaka, Japan) was used to characterize the deformation of the crack-based strain sensor covering the slit wake. The deformation of the nanoscale crack under tensile stress was obtained from in situ TEM tension experiments. The displacement signal was loaded using a homemade stepper motors system and precision micro-displacement stage system with high precision. The vibration signal with specific frequency and amplitude was generated using a vibration generator (JZK-2, Sinocera Piezotronics, Inc., Yangzhou, China). For detecting vibrations with a frequency of 70 Hz, a modal shaker (JZK-2, Sinocera Piezotronics, Inc., China) and a digit multimeter (Keithley, DMM 6500, Cleveland, OH, USA) with a higher sample rate was used. The resistance signal of bio-inspired mechano-sensor was read using a digit multimeter (Keysight, 34465A, Santa Rosa, CA, USA) with Keysight BenchVue software.

3. Results and Discussion

In our slit-based mechano-sensor, the controllable slit was ingeniously used as the mechano-sensory structure. The simulation result shows that the deformation of the solid substrate was mainly concentrated on the slit wake (Figure 1a). Hence, when an alternating load acts on the substrate in the direction perpendicular to the slit length, the slit wake will open and close synchronously with the alternating load. The factors affecting the deformation of the slit wake will be discussed in the follow-up study. The ultrathin strain-sensitive sensing film based on the nanoscale crack array was utilized as the sensing element for converting external mechanical signals into resistance change (Figure 1b–d). The FUCMSS is composed of a flexible substrate, conductive metal layer, electrode and protective layer. Due to the extremely small bending stiffness, the FUCMSS is prone to periodic bending deformations under small alternating loads. In the bending-deformation process, the FUCMSS shows a large change in the electrical resistance, which contributes to the variation of the nanoscale crack width.

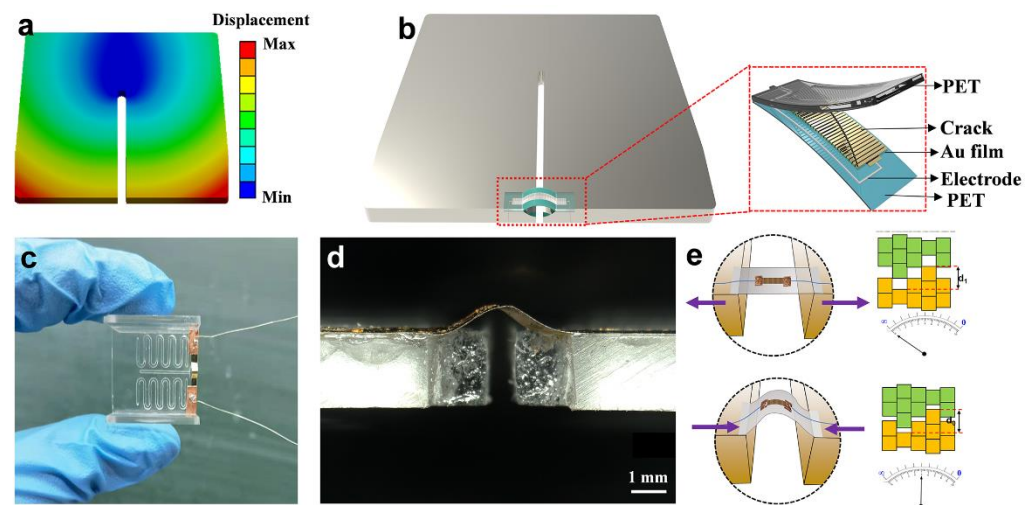


Figure 1. The bio-inspired coupling design of slit-based mechano-sensor composed of FUCMSS and substrate with controlled slit. (a) Finite-element simulation analysis of the substrate with controllable slit. (b) The schematic of the slit-based mechano-sensor. (c) The manufactured slit-based sensor sample. (d) The bending deformation of FUCMSS covering slit wake. (e) The connection–disconnection process of nanoscale cracks with the bending deformation of the FUCMSS.

Crack patterns with jagged crack edges undergo the disconnection–reconnection process in response to mechanical stimuli (Figure 1e) [32]. For example, under tensile stress perpendicular to the crack length, the edges of the cracks are oriented away from each other until the crack edges are completely separated. In this process, the resistance of the FUCMSS increases significantly. Conversely, the resistance of the FUCMSS decreases with the approach of the crack edges. It is also worth noting that the FUCMSS shows different sensitivity to mechanical signal in different bending stages. Specifically, the sensitivity of the sensor is significantly improved with the bending of the FUCMSS from straight to fully folded. Hence, if the sensor begins working from a certain initial bending state, it will possess higher sensitivity than if beginning from a flat state. Here, the coupling design of the slit-based mechano-sensor was carried out. The FUCMSS was used to cover the slit wake with a certain initial bending. With the open and close of the slit wake under alternating loads, the FUCMSS underwent corresponding periodic bending deformations. By combining the deformation characteristic of the slit wake and the ultrathin FUCMSS under alternating loads, the slit-based mechano-sensor showed excellent sensing performance for multiple mechanical signals such as dynamic force, displacement, velocity, acceleration, and so on. Obviously, the deformability of the slit wake in response to low mechanical signals as well as the sensitivity of the FUCMSS are important factors for determining the sensing performance of the slit-based mechano-sensor.

As the sensing element of the slit-based mechano-sensor, the FUCMSS with a nanoscale crack pattern was manufactured using the traditional mechanical bending method (Figure 2a). The cracks were generated on the Au layer with the tensile stress exceeding the fracture toughness of the metal film. Therefore, the direction of the slit length was perpendicular to the direction of the bending forces. Firstly, the nano-thickness Au film was generated on the polyethylene terephthalate (PET) film by controllable physical deposition (Figure 2b). Then the above film was mechanically bent using the home-made instrument. In the bending process, the magnitude and frequency of the tensile stress as well as the bending degree of the sensing film are all important parameters to determine the crack formation. Therefore, with the home-made instrument, the weight was used to apply tensile stress to the film, the frequency of the alternating load was regulated by changing the reciprocating frequency of the stepping motor, and the film was placed on a slender rod to regulate the bending degree of the film. Figure 2c,d clearly indicate that the nanoscale fatigue cracks were formed in the Au layer. Among the many parameters, the density of the crack has a great influence on the

sensitivity of the FUCMSS. In our research, the density of the nanoscale crack was adjusted by changing the radius of the slender rod in Figure 2a. The result indicates that cracks can only be produced when the radius of slender rod is less than 1 mm. With the further decrease in slender-rod radius, the crack density increased significantly. Meanwhile, there was a significant positive correlation between the sensitivity of the FUCMSS and the crack density. Here, the metal slender rod with radius of 0.5 mm was chosen in our research. The dense crack patterns were formed on the Au layer, and the density of crack was about $200/700 \mu\text{m}^2$.

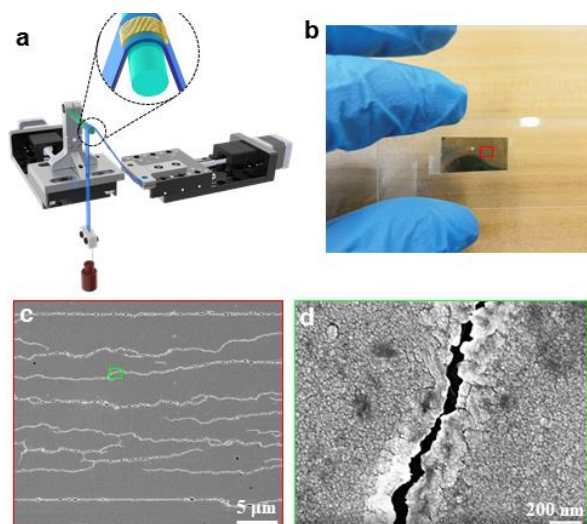


Figure 2. Fabrication of the crack-based flexible strain sensor. (a) The home-made instrument for manufacturing nanoscale crack on flexible PET substrate. (b) The crack-based strain sensor. (c) The nanoscale crack array on the flexible substrate. (d) Local enlarged image taken from (c) denoted by green square.

The performance of the FUCMSS including sensitivity, mechanical stability, and response time were researched in detail. Figure 3a shows the sensing performance of the FUCMSS that was fabricated using different radii of the slender rod. The result indicates that the sensitivity of the FUCMSS to dynamic mechanical signals can be significantly improved by decreasing the bending curvature radius. Figure 3b shows the dynamic $\Delta R/R_0$ response curve of the FUCMSS under different peak strains. The result indicates the variation in resistance of the FUCMSS for different peak strains, in sharp contrast to the original sample without cracks (purple curve). Under different strains, the current–voltage (I–V) curves of the crack-based sample and crack-free bare film are shown in Figure 3c. The strain-sensitive film with microcracks showed a stable increase in electric current with the increase in strain. Therefore, the FUCMSS, which can even sensitively detect a change of 0.1% strain, showed excellent strain-sensing performance. Hysteresis is also one of the important indicators of the strain sensor. As can be seen from Figure 3d, the response time of the FUCMSS was about 93 ms during the mechanical-signal-loading stage, while 112 ms was required to return to the initial state during the unloading process. In addition, the durability of the FUCMSS was also tested. Figure 3e indicates that the resistance value of the sample was relatively stable during the 0–10,000 cycles of alternating load. There was no significant performance degradation. Figure 3f shows the relative resistance of the tensile and release cycles after eight cycles with the change in the strain curve. The sensing curves of the tensile and release cycles in the 1st, 10th, 100th, 500th, 1000th, 2000th and 5000th tensile and release cycles were consistent, indicating that the strain sensor has good monotonicity and long-term stability before failure. In summary, The FUCMSS shows excellent sensitivity, repeatability and tensile durability.

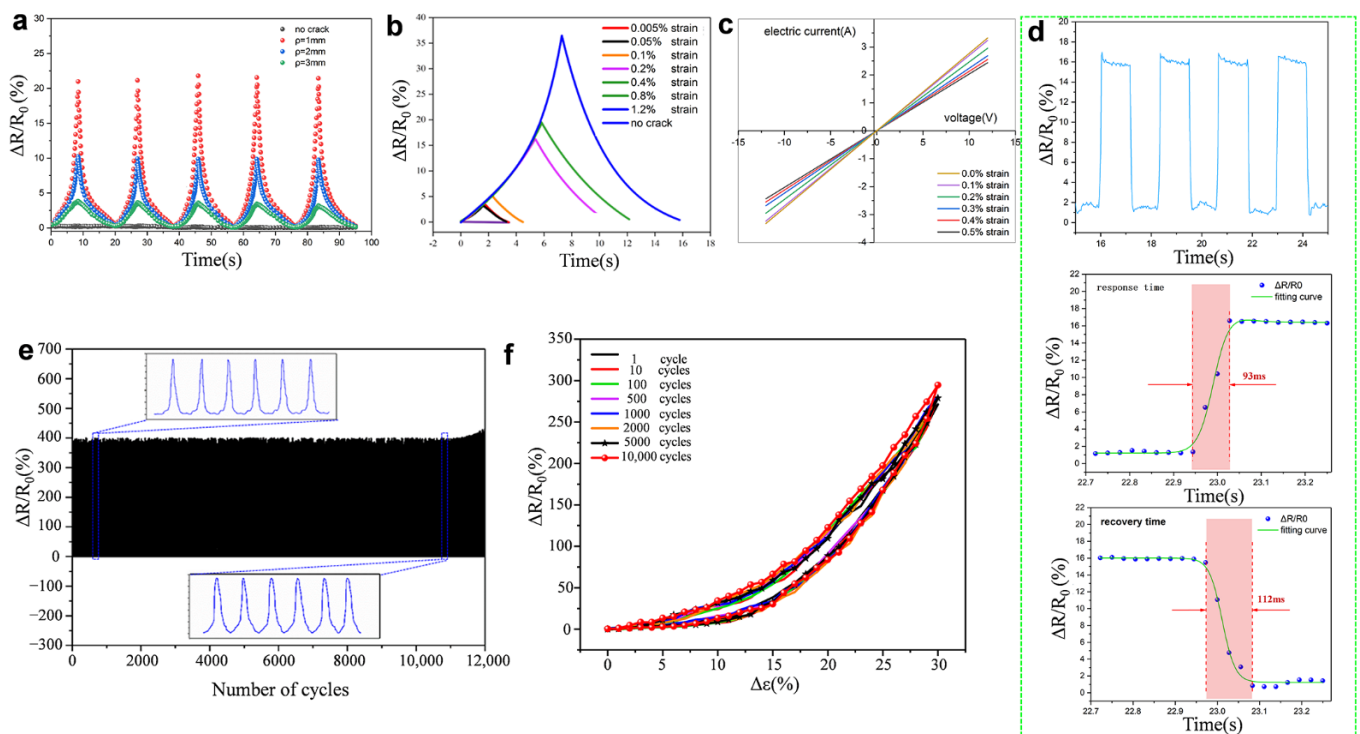


Figure 3. Characterization of the performance of slit-based mechano-sensor. (a) The resistance response of various crack-based strain sensor fabricated using different radii of slender rod. (b) Reversible loading-unloading behavior for various final strains. (c) The current-voltage (I - V) curves of crack-based strain sensor. (d) The response and recovery time of the crack-based strain sensor. (e) Relative resistance change-time curves of strain sensor for 12,000 loading/unloading cycles. (f) The loading-unloading curves at different stages.

The FUCMSS covering the slit wake bends with the open and close of slit. Therefore, to understand the relationship between the different types of bending deformation of the PET substrate and the change in resistance of the Au layer is crucial for optimizing the design of the slit-based mechano-sensor. When compressive stress is applied to the FUCMSS, there will be two different forms of bending deformation: concave bending and convex bending (Figure 4a). The Au layer is located on the upper surface of the PET substrate. Hence, in convex bending, the nanoscale crack width increases with the bending deformation of the FUCMSS, which further leads to an increase in resistance. Conversely, in concave bending, the edges of the cracks are close to each other, resulting in a decrease in resistance. Figure 4b,c show the relative resistance ($\Delta R/R_0$) as a function of strain (ϵ) about the FUCMSS under the conditions of the above two types of bending deformation. The results indicate that in concave-bending mode or convex-bending mode, there is a positive correlation between the value of $\Delta R/R_0$ and the absolute value of ϵ . However, when the FUCMSS had the same absolute value of ϵ , the value of $\Delta R/R_0$ in convex-bending mode was two orders of magnitude higher than the that in the concave-bending mode. Meanwhile, the Au film without the nanoscale crack structure was not sensitive to the bending deformation of the PET substrate. Obviously, the above analysis shows that the FUCMSS working in the convex-bending mode is more sensitive to the bending deformation. Hence, the FUCMSS working in the convex-bending mode has a greater advantage in low-mechanical-signal detection. Additionally, Figure 4c shows that the rate of the change in $\Delta R/R_0$ increases significantly with the increase in bending deformation, indicating that with a certain initial bending, the sensitivity of the FUCMSS can be further improved.

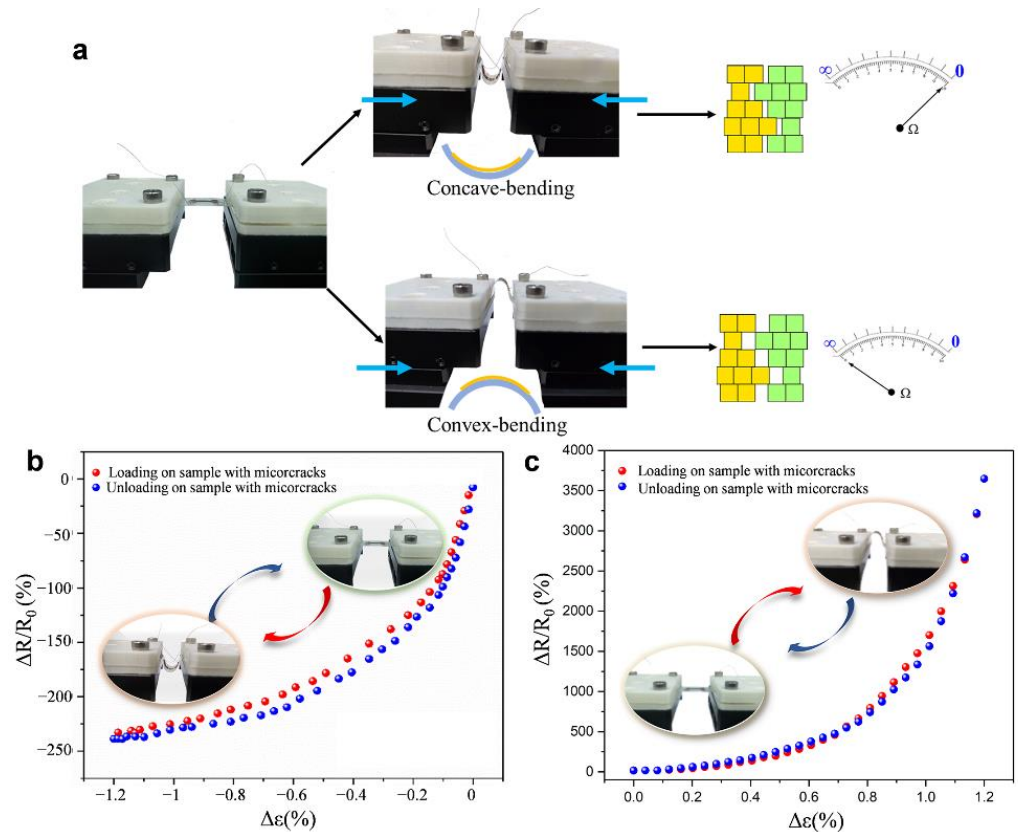


Figure 4. Two different bending-deformation mode of FUCMSS under compressive stress. (a) Two different types of bending deformation of the PET substrate under compressive stress and the corresponding change in resistance. (b) The loading–unloading curve of the FUCMSS under concave-bending deformation. (c) The loading–unloading curve of the FUCMSS under convex-bending deformation.

The deformability of the slit wake in response to low mechanical signals has a great influence on the performance of the slit-based mechano-sensor. Here, the factors affecting the deformability are systematically analyzed. According to the theory of fracture mechanics, the deformation of slit can be represented by [33]:

$$w \approx \frac{(1 + \nu)(3 - \nu)}{2E} Y\sigma \sqrt{a^2 - x^2} \tag{1}$$

Here, w is the width of the slit, ν is Poisson’s ratio, E is the elastic modulus of homogeneous material, Y is the shape factor, σ is the applied stress, the direction of which is perpendicular to the length of the slit, a is the length of slit, x is distance from any point of the slit to the slit wake. At the slit wake, the value of x is 0. The deformation of the slit wake, w_s , can be given by:

$$w_s \approx \frac{(1 + \nu)(3 - \nu)}{2E} Y\sigma a \tag{2}$$

Equation (2) indicates that with the decrease in elastic modulus, E , the deformability of the slit wake can be effectively improved. Many studies have revealed that the “hollowed out” design can significantly reduce the overall stiffness of the structure, E_t , which can be represented by:

$$E_t = E(1 - V_p^2) \tag{3}$$

Here, V_p is the effective removal area of the solid substrate. Therefore, the w_s of the substrate with “hollow out” design can be given by:

$$w_s \approx \frac{(1 + \nu)(3 - \nu)}{2E(1 - V_p^2)} Y\sigma a \tag{4}$$

Compared with Equation (2), Equation (4) clearly indicates that the change in slit width at the slit wake is significantly improved because of the “hollow out” design.

Next, the finite-element-modeling method was used to further verify the effectiveness of “hollow out” design strategy on improving the deformability of the slit wake (Figure 5a–g). Figure 5h further indicates that the w_s of sample g with the maximum effective removal area was significantly higher than that of the other samples. Under the same compressive stress, the slit-wake deformation of sample g was approximately two hundred times greater than the sample without the hollowed-out design. Hence, the hollowed-out structure of sample g was utilized in the next substrate design.

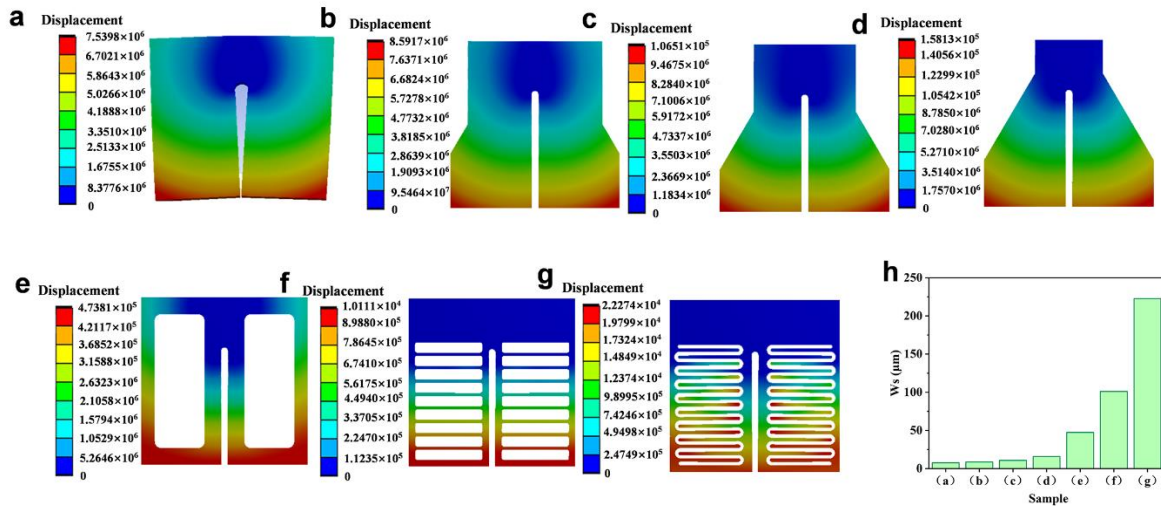


Figure 5. The influence of the effective removal area on the deformation of slit wake. (a–g) Finite-element-simulation analysis of the influence of different “hollow out” structures on the deformation of slit wake. (h) The statistical results of the slit-wake deformation for the samples from (a–g) with different “hollow out” structures.

Equation (4) indicates that slit length, a , has a great influence on the deformation of the slit wake. Figures 6 and 7a show that the deformability of the slit wake was significantly improved with the increase in slit length. Hence, simply considering the deformation demand of the slit wake, increasing the slit length is an efficient strategy. However, the stress concentration at the slit tip, which would lead to the catastrophic failure of the functional structure by inducing crack nucleation due to tip flaws, is also significantly strengthened with the increase in slit length (Figure 7a). Obviously, in comprehensive consideration of the sensitivity as well as the mechanical stability, the slit length can only be moderately increased. In addition, the influence of the solid substrate’s thickness on the deformability of the slit wake was also investigated using the finite-element-modeling method. In order to coincide with the subsequent preparation experiments, polymethylmethacrylate (PMMA) was selected as the constituent material of the substrate. Figure 7b indicates that, with the change in substrate thickness from 1 mm to 8 mm, the deformability of the slit wake decreased slightly. Obviously, the influence of substrate thickness on slit-wake deformability is much less than that of elastic modulus and slit length.

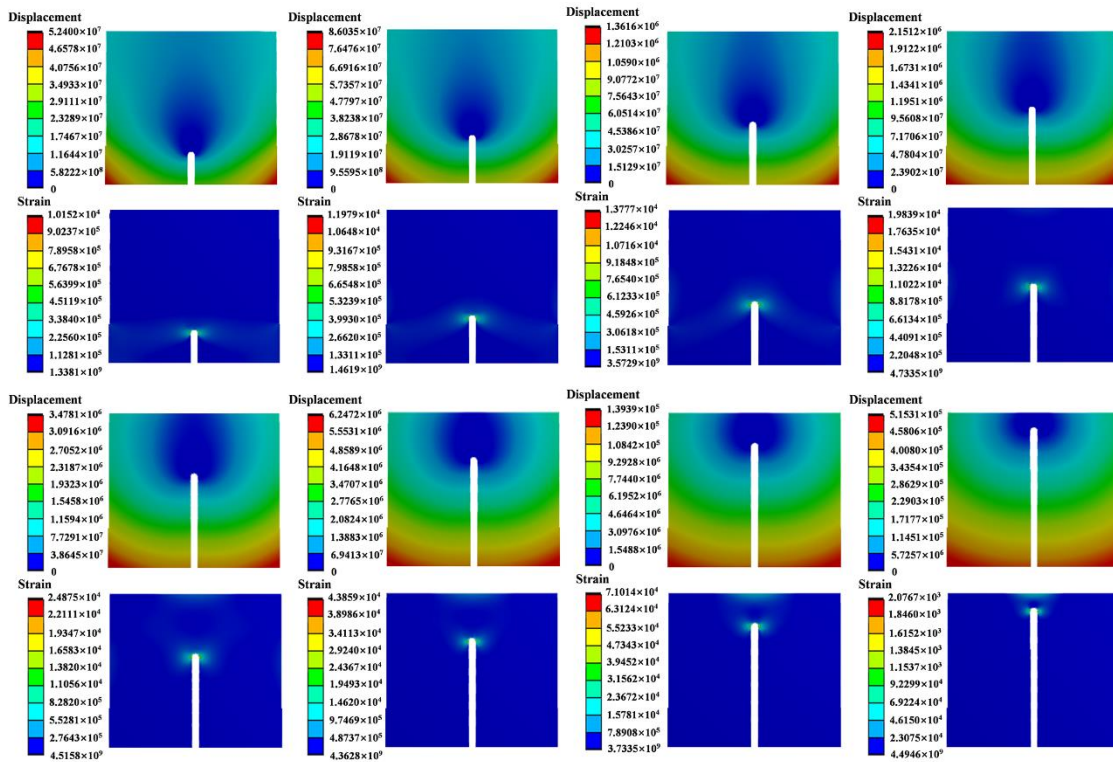


Figure 6. Finite-element-simulation analysis of the influence of slit length on the slit-wake deformation as well as the stress concentration on the slit tip.

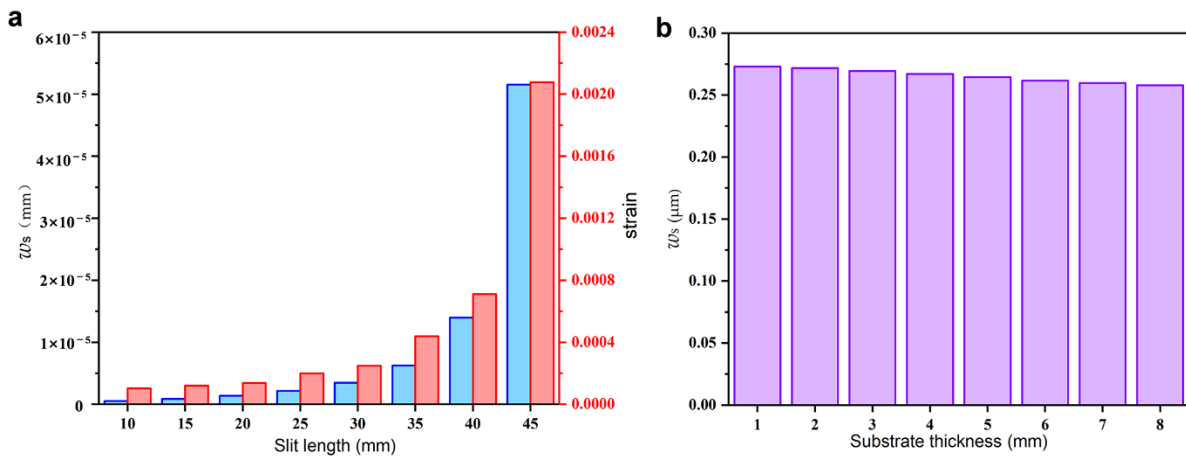


Figure 7. Simulation analysis of the influence of slit length and substrate thickness on the slit-wake deformation. (a) The slit-wake deformation and stress concentration on the slit tip with different slit lengths. (b) The influence of substrate thickness on the slit-wake deformation.

Based on the independent design of the FUCMSS as well as the substrate with the slit, the coupling design of the slit-based mechano-sensor was further carried out. Firstly, the slit was manufactured on the PMMA substrate via laser ablation (Figure 8a). The effective removal area was 400 mm^3 , the E_t of the substrate was about 1.5 GPa, the length of slit was about 15 mm, and the thickness of substrate was about 1 mm. Meanwhile, to improve the deformability of the slit wake, the optimal “hollow out” design strategy in Figure 5g was utilized and processed on the substrate (Figure 8b,c). Then, the FUCMSS in convex-bending mode was bonded to the upper surface of the slit wake (Figure 8d). Figure 8e indicates that when the compressive stress acted on the solid substrate, the height of the FUCMSS arching significantly increased with the decrease in w_s . Meanwhile, the

edges of the nanoscale crack on the Au layer gradually separated, which further led to the increase in resistance (Figure 8f).

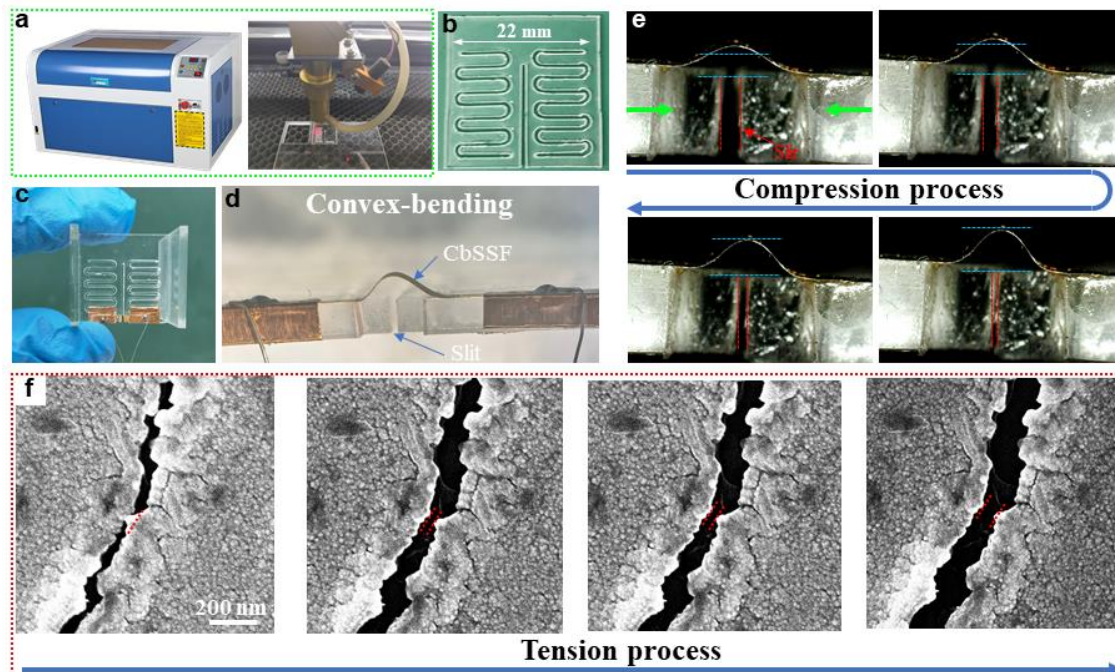


Figure 8. Preparation and characterization of slit-based mechano-sensor. (a) The slit-wake deformation and stress concentration on the slit tip with different slit lengths. (b) The substrate based on the optimal “hollow out” design strategy in Figure 5g. (c) The bio-inspired slit-based mechano-sensor. (d) The FUCMSS covering the slit wake in convex-bending mode. (e) The bending of FUCMSS with the change in slit width. (f) The change in nanoscale crack width with the bending of FUCMSS.

The research on the FUCMSS has revealed that the initial bending degree of the PET substrate has a great influence on the sensitivity to low mechanical signals. Therefore, the bending degree of the FUCMSS was controlled by adjusting the distance from the highest point of the FUCMSS to the upper surface of the substrate. Figure 9a indicates that the heights from sample I to sample IV were 0, 0.44 mm, 0.84 mm, and 1.55 mm, respectively. A compressive force of 0.5 N was applied to the four samples, respectively. The results indicate that the resistance change in the slit-based mechano-sensor was positively correlated with the bending degree of the FUCMSS (Figure 9b). The $\Delta R/R_0$ of sample IV with the maximum bending was about of 1400, while the $\Delta R/R_0$ of sample I with the tiled film was three orders of magnitude smaller than sample IV. In addition, the $\Delta R/R_0$ responses of the four samples under a square wave were compared; the square-wave signal input to the exciter had an amplitude of 1 V and a frequency of 0.5 Hz. Figure 9c also indicates that sample IV had the best waveform-recognition ability for dynamic mechanical signals because of its more significant resistance change. Hence, improving the bending degree of the FUCMSS distributed on the surface of the solid substrate is one of the most important ways to improve the sensitivity of the slit-based mechano-sensor to low mechanical signals. In the next study, sample IV was chosen to evaluate the performance of the slit-based mechano-sensor. In summary, for the solid substrate, the slit length and reasonable “hollow out” design, which influences the overall stiffness of the substrate, are important factors in determining the performance of the slit-based mechano-sensor. Additionally, for the FUCMSS covering the slit wake, the parameters (such as density, length, width, roughness of slit edges) of the slit array as well as the initial bending degree are important factors in determining the performance of the slit-based mechano-sensor.

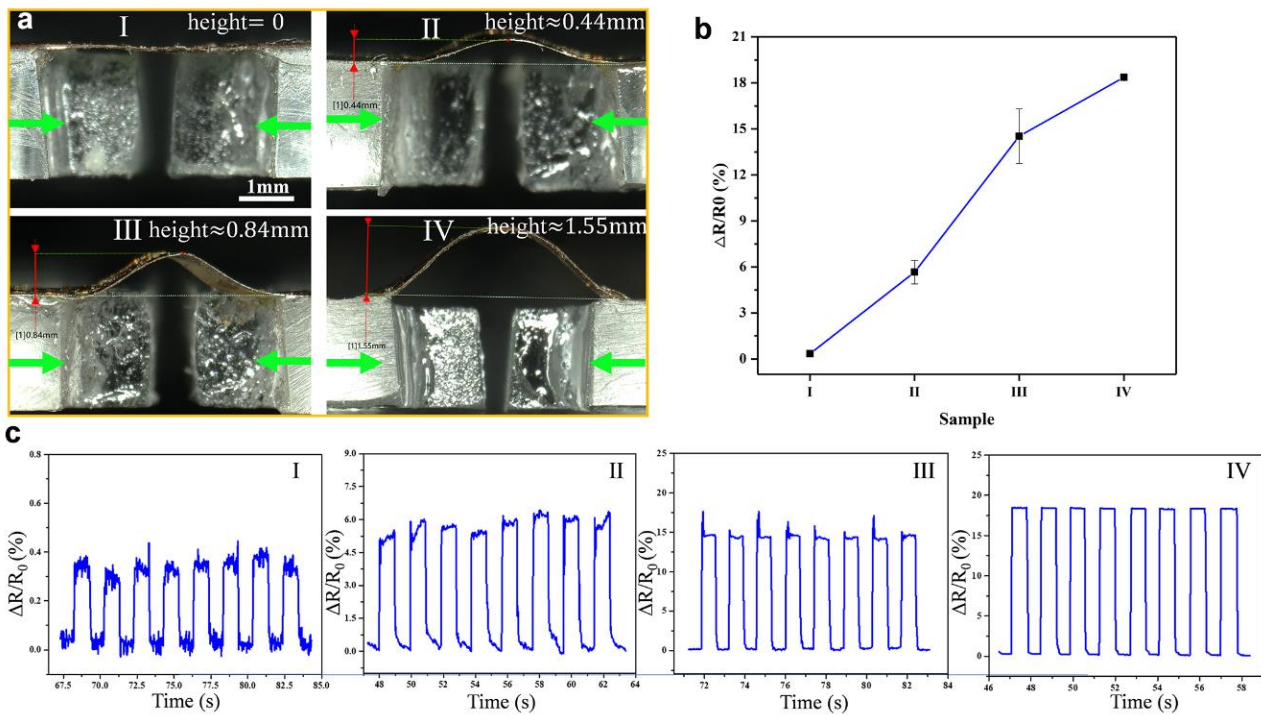


Figure 9. The influence of the initial bending degree of FUCMSS on the sensitivity of slit-based mechano-sensor. (a) The initial bending degree of FUCMSS covering slit wake, the direction of the green arrow represents the direction in which the load is applied. (b) The resistance response of the four samples in (a) in response to the same mechanical stimuli. (c) The dynamic signal-recognition capability of the four samples in (a).

To evaluate the sensing performance of the slit-based mechano-sensor, the impact-response experiment of two small particles falling on the substrate were carried out (Figure 10a). The two particles, which had masses, m , of 0.0345 g and 0.3775 g, were used in the experiment. The falling height of the particles was 10 cm. It is worth noting that the mechano-sensor was placed vertically so that the direction of the impact force was perpendicular to the slit length (Figure 10a). The $\Delta R/R_0$ responses of the slit-based mechano-sensor to the impact signals were compared. Figure 10b indicates that all the impacted signals caused by the above two particles were well detected. Meanwhile, there was a significant positive correlation between the $\Delta R/R_0$ response and particle mass.

In order to further evaluate the ability of the slit-based mechano-sensor to sense small displacement changes, the precision displacement table was used to manually apply a reciprocating displacement signal less than 10 μm (Figure 10c). Figure 10d indicates that the sensor showed a strong response to the above displacement signal. The difference in the $\Delta R/R_0$ peak was caused by manual operation. Meanwhile, the fluctuation and nonlinear increase in $\Delta R/R_0$ caused by the shaking of the hand in the static holding stage is also significantly reflected. The above results indicate that the slit-based mechano-sensor showed excellent sensing performance to the low displacement signal.

Vibration sensors have an important application value in the engineering field. Here, the application of the slit as a mechano-sensory structure in the design of a vibration sensor is further explored. In order to better cooperate with the mass block, the slit was processed on a hollow cylinder instead of a flat substrate. The crack-length direction was parallel to the upper surface of the cylinder. The finite-element-stimulation results show that, with the external load acting vertically on the upper surface of the cylinder, the maximum deformation of the slit tail occurred at the farthest distance from the slit tip (Figure 11a). Therefore, the design strategy of the slit-based mechano-sensor based on a planar substrate is also suitable for a curved substrate. Analogous to the traditional inertial

vibration sensor, a mass block (112.5 g) was placed on the upper surface of the cylinder (Figure 11b). The cylinder was fixedly connected to the tested device with bolts. Therefore, as the cylinder vibrated with the tested device, the relative motion occurred between the mass block and the cylinder, which further led to the compression deformation of the slit wake and the bending deformation of the FUCMSS. Next, the application tests were then performed to evaluate the sensing performance of the vibration sensor for the weak dynamic signal. Firstly, the vibration sensor was fixed to the table and knocking signals with different intensities acted on the desktop. Figure 11c indicates that the knocking signals with different intensities were accurately detected. In addition, to further evaluate the sensing performance of the vibration sensor, the impact signal caused by the ball (12 g) falling from the height of 30 cm onto the desktop was detected. The landing site was 60 cm away from the sensor. Figure 11d shows that the bouncing signal of the ball was detected sensitively. Figure 11d clearly indicates that the impact intensity between the steel ball and desktop rapidly decreased with the increase in bounce times. The above results clearly indicate that the bio-inspired strategy has good application prospects in the design of a vibration sensor.

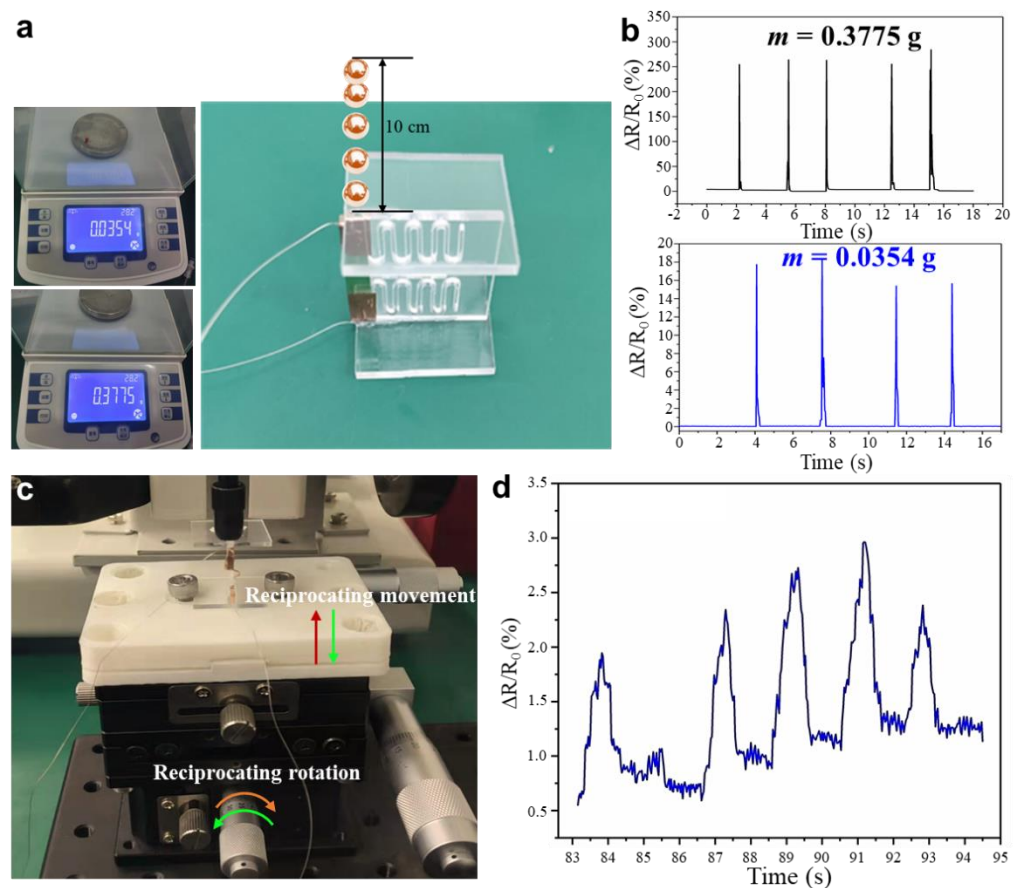


Figure 10. The sensitivity of slit-based mechano-sensor to the dynamic mechanical signal. (a) The impact-response experiment of two small particles falling on the substrate. (b) The resistance response of slit-based mechano-sensor to different impact signals. (c) The displacement loading using a precision displacement table. (d) The resistance response of slit-based mechano-sensor to displacement signal.

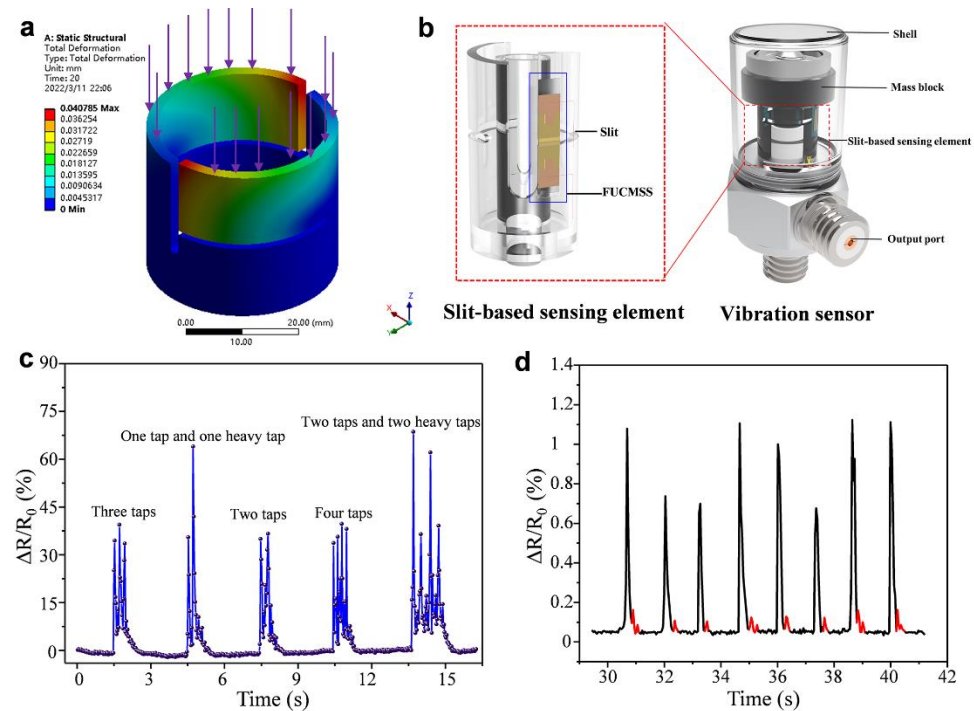


Figure 11. The vibration sensor based on the bio-inspired strategy. (a) The deformation of slit wake in the case of a slit processed on a hollow cylinder. (b) the composition of slit-based vibration sensor. (c) The resistance response of vibration sensor to desktop knocking signal. (d) Detection of mechanical signal generated by the impact between the steel ball and the desktop.

4. Conclusions

In summary, inspired by the coupling deformation characteristic of biological slit-based mechano-sensilla, the internal mechano-sensor using the slit as a sensory structure and flexible strain sensor as a sensing element was designed. To improve the deformability of the slit wake, a hollow structure, which can reduce the compressive stiffness of substrate, was designed. The experimental and theoretical analysis results show that there was a positive correlation between the deformation of the slit wake and the effective removal area of the hollow structure. As the sensing element, the flexible crack-based strain sensor was fabricated and covered the slit wake. The results indicate that the density of the nanoscale fatigue cracks, which have a great influence on the sensitivity of the mechano-sensor, can be controlled at $200/700 \mu\text{m}^2$ by changing the parameters such as the load, loading frequency and bending degree of the substrate. Meanwhile, our research also indicates that improving the initial bending degree of the flexible strain sensor covering the slit wake can significantly improve the sensing performance of mechano-sensor. We also explored the application of the bio-inspired strategy on the design of a vibration sensor. The experimental results show that the vibration sensor can effectively detect the low dynamic mechanical signal such as the dynamic displacement signal and impact signal. It can be expected that such a bio-inspired design strategy will provide an entirely new idea for the internal mechano-sensor to improve the proprioceptive capability of intelligent equipment.

Author Contributions: Conceptualization, K.W. and Q.W.; methodology, K.W. and L.G.; software, Y.G.; validation, K.W. and Z.L.; formal analysis, D.W. and J.L.; investigation, K.W. and L.G.; resources, Q.W.; data curation, K.W. and Y.G.; writing—original draft preparation, K.W., J.L. and Q.W.; writing—review and editing, Q.W.; visualization, L.G.; supervision, K.W.; project administration, K.W. and Q.W.; funding acquisition, K.W. All authors have read and agreed to the published version of the manuscript.

Funding: This work was financially supported by the national natural science foundation of China (52005356) and Postdoctoral Science Foundation of China (Grant No. 2020T130457, 2019M661920). The natural science foundation of Jiangsu Province (BK2020881).

Institutional Review Board Statement: Not applicable.

Informed Consent Statement: Not applicable.

Data Availability Statement: Not applicable.

Conflicts of Interest: The authors declare no conflict of interest.

References

1. Lin, Z.W.; Zhang, G.Q.; Xiao, X.; Au, C.; Zhou, Y.H.; Sun, C.C.; Zhou, Z.H.; Yan, R.; Fan, E.D.; Si, S.B.; et al. A Personalized Acoustic Interface for Wearable Human–Machine Interaction. *Adv. Funct. Mater.* **2021**, *32*, 2109430. [[CrossRef](#)]
2. Liu, Z.Y.; Qi, D.P.; Leow, W.R.; Yu, J.C.; Xiloyannis, M.; Cappello, L.; Liu, Y.Q.; Zhu, B.W.; Jiang, Y.; Chen, G.; et al. 3D-Structured Stretchable Strain Sensors for Out-of-Plane Force Detection. *Adv. Mater.* **2018**, *30*, 1707285. [[CrossRef](#)] [[PubMed](#)]
3. Sengupta, D.; Trap, D.; Kottapalli, A.G.P. Piezoresistive Carbon Nanofiber-Based Cilia-Inspired Flow Sensor. *Nanomaterials* **2020**, *10*, 211. [[CrossRef](#)] [[PubMed](#)]
4. Lu, Y.L.; Zhu, T.; Chen, L.A.; Bao, X.Y. Distributed Vibration Sensor Based on Coherent Detection of Phase-OTDR. *J. Lightwave Technol.* **2010**, *28*, 3243–3249.
5. Nakata, T.; Phillips, N.; Simoes, P.; Russell, I.J.; Cheney, J.A.; Walker, S.M.; Bomphrey, R.J. Aerodynamic imaging by mosquitoes inspires a surface detector for autonomous flying vehicles. *Science* **2020**, *368*, 634–637. [[CrossRef](#)]
6. Li, M.; Pal, A.; Aghakhani, A.; Pena-Francesch, A.; Sitti, M. Soft actuators for real-world applications. *Nat. Rev. Mater.* **2021**, *7*, 235–249. [[CrossRef](#)]
7. Li, Z.J.; Huang, B.; Ajoudani, A.; Yang, C.G.; Su, C.Y.; Bicchi, A. Asymmetric Bimanual Control of Dual-Arm Exoskeletons for Human-Cooperative Manipulations. *IEEE Trans. Robot.* **2018**, *34*, 264–271. [[CrossRef](#)]
8. Aoi, S.; Manoonpong, P.; Ambe, Y.; Matsuno, F.; Worgotter, F. Adaptive Control Strategies for Interlimb Coordination in Legged Robots: A Review. *Front. Neurobotics* **2017**, *11*, 39. [[CrossRef](#)]
9. An, J.; Chen, P.F.; Wang, Z.M.; Berbille, A.; Pang, H.; Jiang, Y.; Jiang, T.; Wang, Z.L. Biomimetic Hairy Whiskers for Robotic Skin Tactility. *Adv. Mater.* **2021**, *33*, 2101891. [[CrossRef](#)]
10. Chen, N.N.; Tucker, C.; Engel, J.M.; Yang, Y.C.; Pandya, S.; Liu, C. Design and characterization of artificial haircell sensor for flow sensing with ultrahigh velocity and angular sensitivity. *J. Microelectromechanical Syst.* **2007**, *16*, 999–1014. [[CrossRef](#)]
11. Alfarhel, A.; Kosel, J. Magnetic Nanocomposite Cilia Tactile Sensor. *Adv. Mater.* **2015**, *27*, 7888–7892. [[CrossRef](#)]
12. Wang, K.J.; Zhang, J.Q.; Song, H.; Fang, Y.Q.; Wang, X.L.; Chen, D.B.; Liu, L.P.; Niu, S.C.; Yao, Z.W.; Han, Z.W.; et al. Highly Efficient Mechano-electrical Energy Conversion Based on the Near-Tip Stress Field of an Antifracture Slit Observed in Scorpions. *Adv. Funct. Mater.* **2019**, *29*, 1807693. [[CrossRef](#)]
13. Vogt, D.M.; Park, Y.L.; Wood, R.J. Design and Characterization of a Soft Multi-Axis Force Sensor Using Embedded Microfluidic Channels. *IEEE Sens. J.* **2013**, *13*, 4056–4064. [[CrossRef](#)]
14. Yeo, J.C.; Liu, Z.J.; Zhang, Z.Q.; Zhang, P.; Wang, Z.P.; Lim, C.T. Wearable Mechanotransduced Tactile Sensor for Haptic Perception. *Adv. Mater. Technol.* **2017**, *2*, 1700006. [[CrossRef](#)]
15. Truby, R.L.; Wehner, M.; Grosskopf, A.K.; Vogt, D.M.; Uzel, S.G.M.; Wood, R.J.; Lewis, J.A. Soft Somatosensitive Actuators via Embedded 3D Printing. *Adv. Mater.* **2018**, *30*, 1706383. [[CrossRef](#)]
16. Tapia, J.; Knoop, E.; Mutny, M.; Otaduy, M.A.; Bacher, M. MakeSense: Automated Sensor Design for Proprioceptive Soft Robots. *Soft Robot.* **2020**, *7*, 332–345. [[CrossRef](#)]
17. Kottapalli, A.G.P.; Bora, M.; Asadnia, M.; Miao, J.; Venkatraman, S.S.; Triantafyllou, M. Nanofibril scaffold assisted MEMS artificial hydrogel neuromasts for enhanced sensitivity flow sensing. *Sci. Rep.* **2016**, *6*, 19336. [[CrossRef](#)]
18. Nawi, M.N.M.; Manaf, A.A.; Arshad, M.R.; Sidek, O. Development of microfluidic based multidirectional flow sensor inspired from artificial cupula. *Microsyst. Technol.-Micro-Nanosystems-Inf. Storage Processing Syst.* **2015**, *21*, 1513–1521. [[CrossRef](#)]
19. Qualtieri, A.; Rizzi, F.; Epifani, G.; Ernits, A.; Kruusmaa, M.; De Vittorio, M. Parylene-coated bioinspired artificial hair cell for liquid flow sensing. *Microelectron. Eng.* **2012**, *98*, 516–519. [[CrossRef](#)]
20. Van Meerbeek, I.M.; De Sa, C.M.; Shepherd, R.F. Soft optoelectronic sensory foams with proprioception. *Sci. Robot.* **2019**, *3*, eaau2489. [[CrossRef](#)]
21. Li, C.; Sanchez, R.V.; Zurita, G.; Cerrada, M.; Cabrera, D.; Vasquez, R.E. Gearbox fault diagnosis based on deep random forest fusion of acoustic and vibratory signals. *Mech. Syst. Signal Process.* **2016**, *76–77*, 283–293. [[CrossRef](#)]
22. Fratzl, P.; Barth, F.G. Biomaterial systems for mechanosensing and actuation. *Nature* **2009**, *462*, 442–448. [[CrossRef](#)]
23. Hossli, B.; Bohm, H.J.; Schaber, C.F.; Rammerstorfer, F.G.; Barth, F.G. Finite element modeling of arachnid slit sensilla II. Actual lyriform organs and the face deformations of the individual slits. *J. Comp. Physiol. A: Sensory Neural Behav. Physiol.* **2005**, *195*, 881–894. [[CrossRef](#)]
24. Brownell, P.; Farley, R.D. Orientation to vibrations in sand by the nocturnal scorpion *Paruroctonus mesaensis*: Mechanism of target localization. *J. Comp. Physiol.* **1979**, *131*, 31–38. [[CrossRef](#)]

25. Young, S.L.; Chyasnavichyus, M.; Erko, M.; Barth, F.G.; Fratzl, P.; Zlotnikov, I.; Politi, Y.; Tsukruk, V.V. A spider's biological vibration filter: Micromechanical characteristics of a biomaterial surface. *Acta Biomater.* **2014**, *10*, 4832–4842. [[CrossRef](#)]
26. McConney, M.E.; Schaber, C.F.; Julian, M.D.; Barth, F.G.; Tsukruk, V.V. Viscoelastic nanoscale properties of cuticle contribute to the high-pass properties of spider vibration receptor. *J. R. Soc. Interface* **2007**, *04*, 1135–1143. [[CrossRef](#)]
27. Schaber, C.F.; Gorb, S.N.; Barth, F.G. Force transformation in spider strain sensors: White light interferometry. *J. R. Soc. Interface* **2012**, *09*, 1254–1264. [[CrossRef](#)]
28. Wang, K.J.; Zhang, J.Q.; Liu, L.P.; Chen, D.B.; Song, H.L.; Wang, Y.L.; Niu, S.C.; Han, Z.W.; Ren, L.Q. Vibrational Receptor of Scorpion (*Heterometrus petersii*): The Basitarsal Compound Slit Sensilla. *J. Bionic Eng.* **2019**, *16*, 76–87. [[CrossRef](#)]
29. Erko, M.; Younes-Metzler, O.; Rack, A.; Zaslansky, P.; Young, S.L.; Milliron, G.; Chyasnavichyus, M.; Barth, F.G.; Fratzl, P.; Tsukruk, V.; et al. Micro- and nano-structural details of a spider's filter for substrate vibrations: Relevance for low-frequency signal transmission. *J. R. Soc. Interface* **2015**, *15*, 20141111. [[CrossRef](#)]
30. Wang, K.J.; Zhang, J.Q.; Fang, Y.Q.; Chen, D.B.; Liu, L.P.; Han, Z.W.; Ren, L.Q. Micro/nano-scale Characterization and Fatigue Fracture Resistance of Mechanoreceptor with Crack-shaped Slit Arrays in Scorpion. *J. Bionic Eng.* **2019**, *16*, 410–422. [[CrossRef](#)]
31. Wang, Q.; Fan, C.; Gui, Y.C.; Lu, Y.; Wang, K.J. The Balance Strategy between Structural Safety and Sensing Accuracy Inspired by Slit-Based Mechanical Sensilla. *Appl. Sci.* **2021**, *10*, 8778. [[CrossRef](#)]
32. Zhang, C.; Sun, J.; Lu, Y.; Liu, J.S. Nanocrack-based strain sensors. *J. Mater. Chem.* **2021**, *9*, 754–772. [[CrossRef](#)]
33. Naleway, S.E.; Porter, M.M.; McKittrick, J.; Meyers, M.A. Structural Design Elements in Biological Materials: Application to Bioinspiration. *Adv. Mater.* **2015**, *27*, 5455–5476. [[CrossRef](#)] [[PubMed](#)]